Erosion rates as a potential bottom-up control of forest structural characteristics in the Sierra Nevada Mountains

Ecology, 96(1), 2015, pp. 31–38

Erosion rates as a potential bottom-up control of forest structural characteristics in the Sierra Nevada Mountains

David T. Milodowski,[1] Simon M. Mudd, and Edward T. A. Mitchard

School of GeoSciences, University of Edinburgh, Edinburgh, United Kingdom

Abstract. The physical characteristics of landscapes place fundamental constraints on vegetation growth and ecosystem function. In actively eroding landscapes, many of these characteristics are controlled by long-term erosion rates: increased erosion rates generate steeper topography and reduce the depth and extent of weathering, limiting moisture storage capacity and impacting nutrient availability. Despite the potentially important bottom-up control that erosion rates place on substrate characteristics, the relationship between the two is largely unexplored. We investigate spatial variations in aboveground biomass (AGB) across a structurally diverse mixed coniferous/deciduous forest with an order of magnitude erosion-rate gradient in the Northern Californian Sierra Nevada, USA, using high resolution LiDAR data and field plots. Mean basin slope, a proxy for erosion rate, accounts for 32% of variance in AGB within our field area ($P < 0.001$), considerably outweighing the effects of mean annual precipitation, temperature, and bedrock lithology. This highlights erosion rate as a potentially important, but hitherto unappreciated, control on AGB and forest structure.

Key words: biogeomorphology; biomass; ecological succession; erosion; landscape evolution; LiDAR; mixed-conifer forest; Sierra Nevada; topography.

Introduction

Geomorphic processes act to generate, erode, and redistribute sediment, sculpting the landscape and creating the physical template on which ecosystems develop (Urban et al. 2000, Chase et al. 2012, Detto et al. 2013). In addition, vegetation is an important geomorphic agent, playing a direct role in soil production and modifying the efficacy of erosion and sediment transport (Gabet et al. 2003, Gabet and Mudd 2010, Roering et al. 2010). Life and landscape are thus intimately linked; their coevolution is connected by the interplay between erosion and sediment transport, chemical weathering, hydrology, ecology, and biology.

It is widely documented that elevation-dependent variations in precipitation and temperature place important controls on ecosystem development and functioning in mountain environments. In the Californian Sierra Nevada, USA, these "top-down" controls are manifest in the macroscale altitudinal zonation of ecosystems, primary productivity, and evapotranspiration (Stephenson 1998, Bales et al. 2011, Goulden et al. 2012). In contrast, "bottom-up" controls imposed by the geomorphic evolution of landscapes have received significantly less attention, yet the balance between uplift and geomorphic processes determines the distribution of elevations in a landscape. In addition, geomorphic processes play a key role in determining the thickness, chemistry, and texture of soils, the substrate upon which ecosystems develop (Kirkby 1985, Heimsath et al. 1997, 2012, Dixon et al. 2012, Vanwalleghem et al. 2013).

In actively eroding landscapes, rates of erosion are typically paced by fluvial incision, which sets the lower base-level of adjacent hillslopes (Gilbert 1909, Roering et al. 1999). In response to increased fluvial incision, hillslopes steepen, raising the rate at which sediment is transmitted across hillslopes into the channel network. On steeper hillslopes, gravitational forces begin to overcome resisting forces and sediment transport increases rapidly, limiting further development of hillslope relief (Roering et al. 1999, 2001). Erosion rates not only control the distribution of elevation and topographic gradient across a landscape, they also can control soil texture and chemistry by modulating soil residence time. Minerals in rapidly eroding landscapes spend less time in the soil than minerals in slowly eroding landscapes, thus limiting their exposure to weathering and reducing the potential for clay formation (Mudd and Yoo 2010). There is a strong feedback between erosion rate and residence time, because not only do minerals move through rapidly eroding soils more quickly, but in addition, rapidly eroding soils are thinner than slowly eroding soils (Heimsath et al. 1997). Thus, erosion rates are directly tied to both moisture storage capacity (Graham et al. 2010) and the bioavailability of key nutrients (Vitousek et al. 2003, Porder et al. 2007, Hilton et al. 2013). Given that the establishment of forest communities is fundamentally dependent on the presence of a hospitable substrate from which

Manuscript received 8 April 2014; revised 13 August 2014; accepted 10 September 2014. Corresponding Editor: J. B. Yavitt.

[1] E-mail: d.t.milodowski@ed.ac.uk

vegetation can extract moisture and nutrients, long-term erosion rates may place important controls on forest characteristics; however, the relationship between forest structure, AGB, and erosion rate is largely unexplored.

In this contribution, we use airborne Light Detection and Ranging (LiDAR) data to investigate spatial variations of AGB in a mixed-conifer forest in the Californian Sierra Nevada. Rates of erosion in this landscape vary spatially by an order of magnitude, providing a natural laboratory for investigating the role of changing erosion rates on land surface dynamics. This has motivated a significant body of geomorphological and geochemical research at the site (Riebe et al. 2000, 2001, Yoo et al. 2011, Hurst et al. 2012, 2013), providing a rich knowledge base from which to explore landscape-scale controls on ecosystem properties.

Study Site

Located in the northwestern Sierra Nevada Mountains, California, the field site comprises 83 km^2 of mixed-conifer forest (dominated by *Pseudotsuga menziesii*, *Pinus ponderosa*, *Calocedrus decurrens*, *Pinus lambertiana*, and *Quercus kelloggii*), predominately within the boundaries of the Plumas National Forest (Fig. 1a). The modern climate is strongly seasonal; maximum monthly temperatures range from 9°C to 30°C, and minimum monthly temperatures range from −1°C to 12°C. Annual precipitation is ~1750 mm, with >90% falling between October and April, much of this as snow (data from the PRISM Climate Group at Oregon State University, Corvallis, Oregon, USA; *available online*).[2] Summer moisture balances represent important limitations in ecosystem productivity under seasonally dry climates (Hubbert et al. 2001, Witty et al. 2003); periodic dry-season fires are an important additional factor in driving ecosystem turnover, the most recent of which was the 2008 Scotch Fire, which affected a significant area on the eastern side of the field site.

Draining from the high Sierras, the Middle Fork Feather River incises into bedrock comprising granite and granodiorite plutons as well as metamorphosed volcanic and sedimentary rocks (Saucedo and Wagner 1992). The landscape is composed of incised gorges near the Middle Fork Feather River and its larger tributaries, dissecting a lower-relief plateau (Fig. 1b). Erosion rates calculated from ^{10}Be concentrations in detrital river silts show an order-of-magnitude difference in erosion rates across the landscape, from 20–40 mm/ka (kilo annum) on the plateau surface to >250 mm/ka in the high-relief topography adjacent to the actively incising channels (Riebe et al. 2000, Hurst et al. 2012).

Methods

Airborne LiDAR acquisition (September 2008) and processing were carried out by the National Center for Airborne Laser Mapping, giving a point cloud with an average point density of 9.8 points/m^2, which was interpolated to a 1-m resolution digital elevation model (DEM) of the ground surface. LiDAR can be readily used to quantify the spatial distribution of AGB by exploiting the natural allometric scaling of stem AGB with tree size (e.g., Lefsky et al. 1999). We mapped the mean return height (MRH), which combines information on both canopy height and canopy cover, for all returns within a moving 10-m-radius window (Fig. 2a). Simple canopy metrics like this have been shown to be excellent predictors of AGB (Asner et al. 2012).

In order to calibrate the AGB estimates, we undertook 31 tree inventory plots during the summers of 2012 and 2013, each with a 10 m radius. For each plot, we recorded the species and diameter at breast height (1.3 m), dbh, for all trees with dbh >10 cm. AGB estimates for the field plots were obtained using previously published allometric equations relating dbh to AGB (Appendix: Table A1; Jenkins et al. [2003], Návar [2009]; see also equation 1060 in the Pacific Northwest Plant Biomass Component Equation Library, *available online*).[3] Since there are significant sources of uncertainty in both LiDAR-derived metrics (Mascaro et al. 2011) and plot-based biomass estimates (Chave et al. 2004), we used standardized major axis (SMA) regression to fit a linear model to the data (Warton et al. 2006; Fig. 2b). The regression is fixed through the origin, justified because a plot with no return heights above ground level will have zero AGB. We employ a simple linear model, as the calibration data do not support the use of a more complex parameterization. Uncertainties in both field plot-based biomass and LiDAR-derived canopy metrics were estimated using a Monte Carlo framework (Gonzalez et al. 2010, Yanai et al. 2010), but these uncertainty estimates are not used to weight the regression, due to the fact that they are poorly constrained, and errors in the allometric relationships are likely to have significant bias. One outlier is excluded from the regression analysis (marked as a hollow symbol in Fig. 2b), as the plot biomass was skewed by the presence of one very large tree (*Quercus decurrens*, dbh >1m).

In order to explore the relationship between erosion rate and AGB, we compare aggregated characteristics of second-order drainage basins (defined by Strahler stream order; Appendix), where the channel network is defined using the method outlined by Clubb et al. (2014). Basins with catchments smaller than 20 000 m^2 are excluded from our analysis. We use mean basin slope as a proxy for locally averaged erosion rate: all else being equal, higher erosion rates will generate steeper topography (Ahnert 1970). The functional relationship between mean basin slope and erosion rate is nonlinear (Montgomery and Brandon 2002): mean basin slopes

[2] http://www.prismclimate.org

[3] http://andrewsforest.oregonstate.edu/data/abstract.cfm?dbcode=TP072

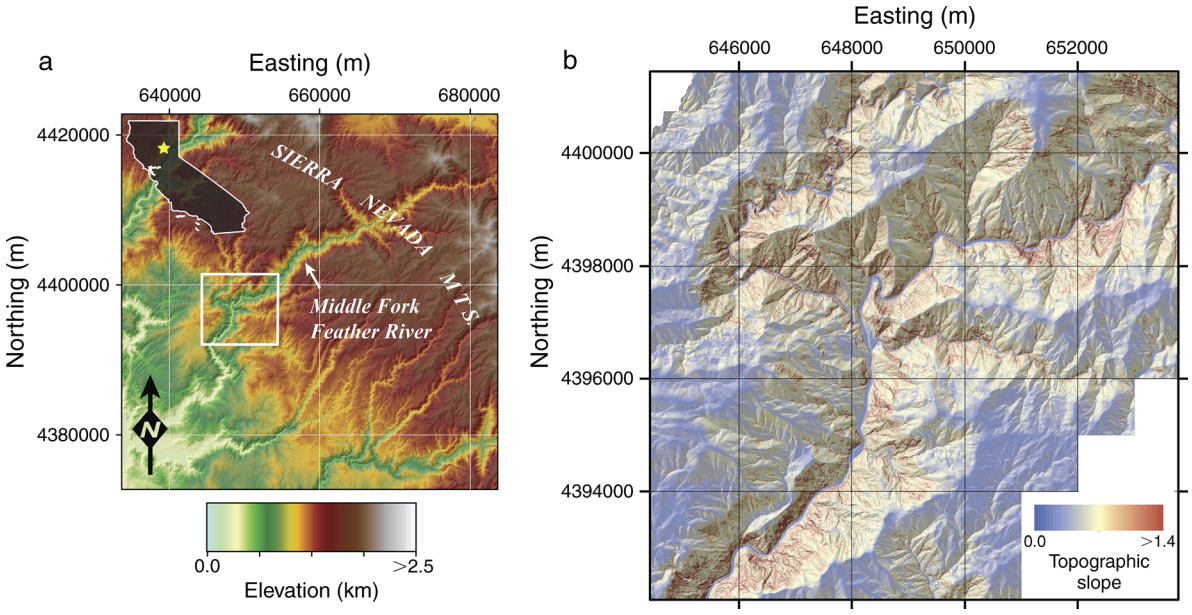

FIG. 1 (a) Location map; the site is located in the Northern Californian Sierra Nevada, USA (see upper-left inset, site indicated by the star). The extent of the study area is indicated by the white box. (b) A map of dimensionless topographic gradient across the study site. Elevated incision along the trunk channel of the Feather River and principal tributaries has driven a steepening of hillslope gradients. The coordinate system for both maps is UTM Zone 10N.

become increasingly insensitive to erosion rates as hillslope gradients steepen toward the threshold of stability and gravitational forces begin to overcome resisting forces, limiting the further development of relief (Roering et al. 1999). Nevertheless, a comparison of mean basin slope and cosmogenic-radionuclide-derived erosion rates in the Feather River region by Hurst et al. (2012) indicates that mean basin slope remains a sensitive metric across the range of erosion rates observed here, and is therefore sufficient to illustrate the erosion gradient in our analysis.

Climate also has a significant influence on forest characteristics in the Sierra Nevada (Stephenson 1998, Urban et al. 2000, Franklin 2003). It is therefore important to take into account local climate gradients within the field site. To achieve this, we utilized 800-m

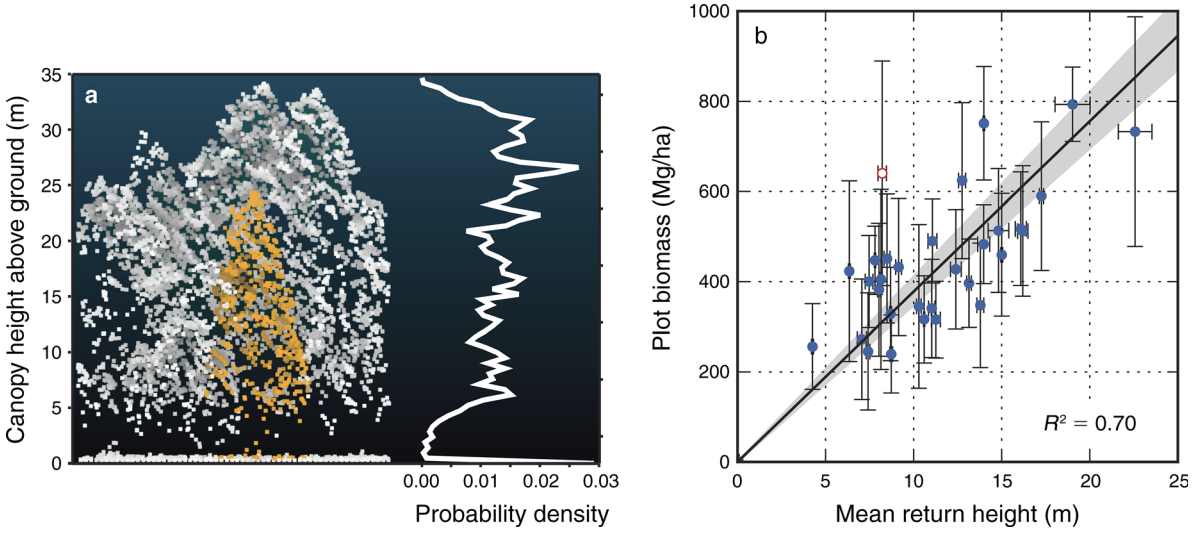

FIG. 2 (a) A view of the LiDAR point cloud extracted for one of the field inventory plots and corrected for topography, so that the point elevations reflect canopy height above ground, alongside the corresponding LiDAR return profile. (b) Plot-based biomass estimates for 31 (0.031 ha) field inventory plots, and mean return height (MRH) of the corresponding return profile. The black line indicates the standardized-major-axis-fitted trend, forced through the origin; the gray region indicates the 95% confidence intervals. The hollow data point indicates an outlier, which was excluded from the regression.

resolution maps of mean annual precipitation (MAP) and mean annual temperature (MAT) from the PRISM Climate Group (see footnote 2; see also Daly et al. 2008). In order to take into account variations in microclimate generated by topography, we downscaled these maps following the method described by Chorover et al. (2011). Soil characteristics can also influence plant community composition and growth; to account for soil parent material, we divided the catchments into two principal bedrock lithologies; granodiorite and meta-volcanic/peridotite. We then used a general linear model (GLM) framework to explore the relative importance of erosion rate (mean basin slope), climate, and bedrock lithology in driving the observed distribution of AGB.

The region was affected by the Scotch Fire in 2008, six months prior to the LiDAR acquisition. In order to test for bias in the results due to the influence of the recent fire, we repeated the analysis using USFS burn-intensity maps to exclude parts of the forest that suffered significant damage to the structurally dominant vegetation (moderate/high intensity; Miller and Thode 2007). A full description of our methods is given in the Appendix.

Results

A comparison of the LiDAR-derived AGB estimates against the field plot AGB estimates yields an R^2 value of 0.70 and a root mean squared error (RMSE) of 103.3 Mg/ha (Fig. 2b). Comparing the distribution of AGB produced by extending the analysis across the study region (Fig. 3a) against the distribution of slopes (Fig. 1b), some important features stand out: (1) a general trend of high biomass on the plateau and lower AGB on steeper, more rapidly eroding topography, (2) the presence of weak aspect-driven variations in AGB, and (3) the AGB distribution on the plateau is disrupted by a series of low-AGB patches, often with sharp, quasi-geometric boundaries, where there has been recent active logging. The latter is likely to add significant scatter to basin-averaged AGB for low gradient basins draining the plateau.

The results from the GLM analysis (Table 1, Appendix: Tables A2 and A3) reveal that mean basin slope, temperature, and precipitation can together explain 44% of the variance in AGB observed in this landscape ($F_{7,278} - 32.9$, $P < 0.001$, $N = 287$). A comparison of single-variable regressions indicates that of these variables, mean basin slope produces the strongest correlation with AGB at the scale of second-order basins, accounting for 73% of this explanatory power (Fig. 3b–e). Accounting for bedrock lithology typically explains a further 2% of the variance in a given model: granodiorite basins tend to have lower biomass than their meta-volcanic counterparts. A comprehensive tabulation of the GLM results is provided in Appendix: Tables A2 and A3. Adding extra terms into the GLM analysis generated incremental improvements to model fit, with no unexpected deviations in model behavior. Importantly, the trends between mean basin slope and AGB are sufficiently strong that even including the regions severely affected by the 2008 fire, there is no major change in the relationship (R^2 for the univariate model changes from 0.32 to 0.34; parameters within standard error). Note that as both the climate and erosion gradients are at least partly topographically structured, a degree of autocorrelation of variables is unavoidable (Pearson's correlation coefficients: mean basin slope–MAT = −0.02; mean basin slope–MAP = −0.40; MAP–MAT = −0.14).

Discussion

The strong negative correlation between mean basin slope and basin-averaged biomass (Fig. 3) suggests that there is an important coupling between hillslope erosion rates and the process of succession and development of plant communities in this region. While the simple linear models assumed in our analysis are likely an oversimplification of the true functional relationships between the variables, the models that explicitly incorporate the influence of erosion rate through spatial variations in mean basin slope perform significantly better than those without. The strength of the trends observed is remarkable given the degree of natural heterogeneity that one might expect, particularly as some parts of the plateau have been logged for timber, which is likely to have reduced the observed correlation. Erosion rates could influence AGB through a variety of mechanisms, but the most likely explanation we believe relates to its influence on the depth of soil and saprolite, and through this water storage and availability for plants.

In the Feather River region, previous work has focused on the geomorphological and geochemical evolution of the landscape. Hurst et al. (2012) observed that in response to increased fluvial incision at their base, hillslopes steepen and become increasingly planar, focusing curvature at the ridge crest, consistent with theoretical and experimental models of nonlinear hillslope sediment transport (Roering et al. 1999, 2001). Decreasing residence times of material within the critical zone across this same transition are indicated by a decrease in the extent of weathering of both saprolite and soil (Riebe et al. 2001, Yoo et al. 2011) and a corresponding drop in the soil clay content (Yoo et al. 2011), again in agreement with theoretical (e.g., Mudd and Yoo 2010) and empirical observations from other rapidly eroding sites in California (Dixon et al. 2012).

The change in residence time of material as it passes through the weathering zone is critical to understanding the functional link between erosion rate and biomass distribution in this setting. In the upland Sierra Nevada, water is the limiting factor in ecosystem productivity (Urban et al. 2000). Mixed-conifer forests are typically established on relatively thin soils overlying strongly weathered saprolite (Hubbert et al. 2001, Witty et al. 2003). Weathered granitic saprolite has an available water capacity of ~12%, which, while lower than that of

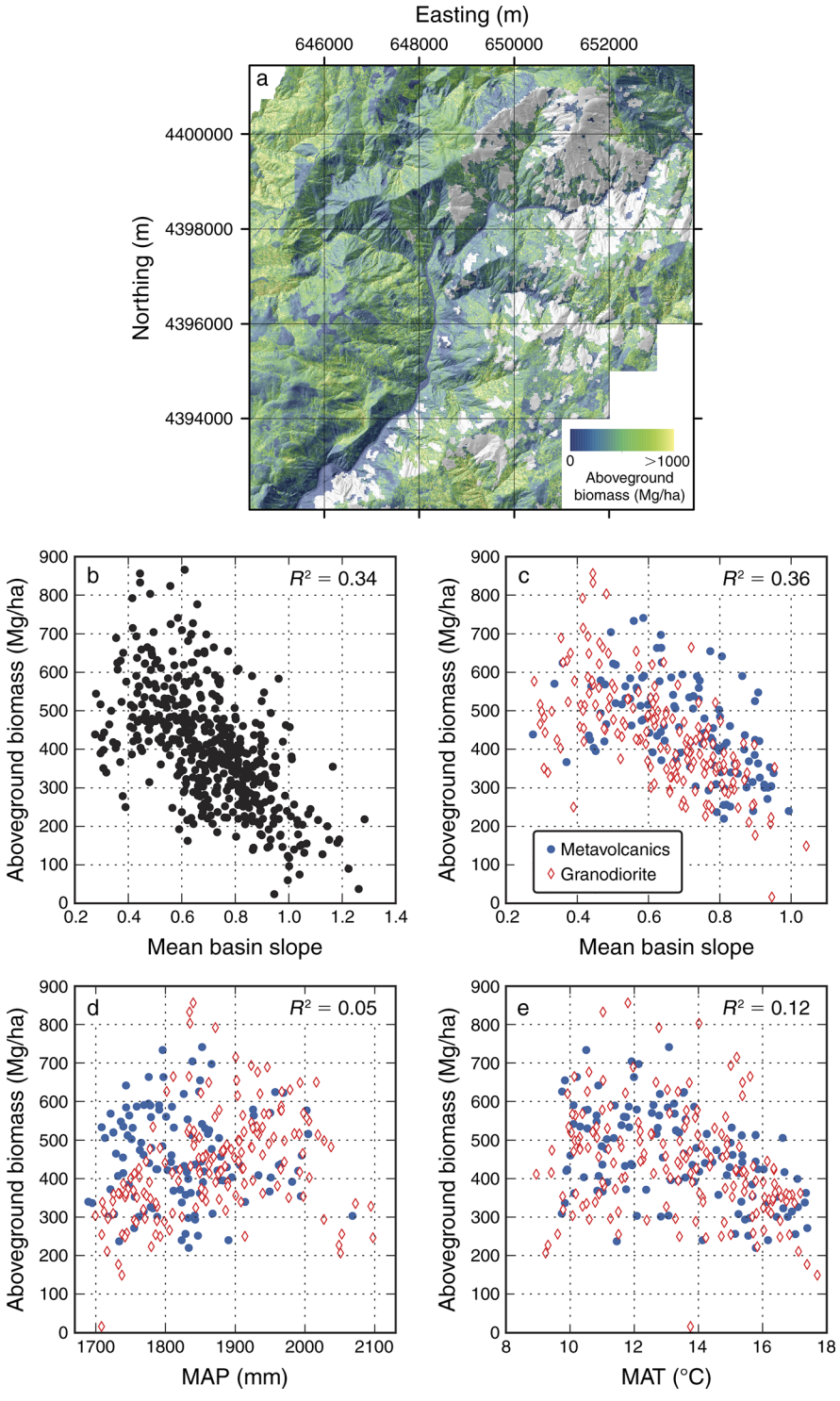

FIG. 3 (a) A map showing the distribution of aboveground biomass, estimated using the calibrated LiDAR metric. Areal extent is identical to Fig. 2b. Regions with no data (gray) indicate regions that suffered moderate-severe burn severity (as defined by Miller and Thode [2007]) in the 2008 Scotch Fire. Logged areas on the plateau are visible as uniformly low biomass patches, often with sharp boundaries. The coordinate system is UTM Zone 10N. (b) Estimated AGB plotted against mean basin slope for all second-order basins with catchment areas >20 000 m^2. (c–e) AGB plotted against (c) mean basin slope, (d) mean annual precipitation (MAP), and (e) mean annual temperature (MAT) for those same basins, but filtered to exclude areas which suffered moderate-to-high-severity burn damage in 2008. Results are shown for the two principal bedrock lithologies present in the study; granodiorite and meta-volcanic/peridotite. Basins for which more than 50% of the area was affected were also removed. Note that including the burned areas do not affect the overall trends.

TABLE 1 Results from nine different general linear model (GLM) analyses exploring the controls on the variation of mean aboveground biomass (AGB) for all second-order drainage basins within the study region.

GLM analysis	Model	Number of basins	R^2	F	df	P
1	AGB ~ MBS	374	0.34	194.6	1, 372	$<2.2 \times 10^{-16}$
2	AGB ~ MBS × MAP × MAT	374	0.47	47.68	7, 366	$<2.2 \times 10^{-16}$
3	AGB ~ MBS	287	0.32	137.2	1, 285	$<2.2 \times 10^{-16}$
4	AGB ~ MAP	287	0.04	12.8	1, 285	0.0004
5	AGB ~ MAT	287	0.12	40.4	1, 285	8.1×10^{-10}
6	AGB ~ MBS × MAP	287	0.39	60.6	3, 283	$<2.2 \times 10^{-16}$
7	AGB ~ MBS × MAT	287	0.35	51.9	3, 283	$<2.2 \times 10^{-16}$
8	AGB ~ MAP × MAT	287	0.18	22.3	3, 283	5.5×10^{-16}
9	AGB ~ MBS × MAP × MAT	287	0.44	32.9	7, 278	$<2.2 \times 10^{-16}$

Notes: Analyses 1 and 2 used the full data set; for all other models, the analysis excluded areas that suffered moderate-severe (as defined by Miller and Thode [2007]) canopy disturbance during the 2008 Scotch Fire, and completely excluded basins for which the affected area accounted for >50% of the total catchment area. R^2 is adjusted. Model components include mean basin slope (MBS), mean annual precipitation (MAP), and mean annual temperature (MAT). A tabulation of all the GLM models explored is given in Appendix: Table A2, alongside a comprehensive breakdown of the respective parameter sets in Appendix: Table A3.

soil (~20%), makes it a vital water store that continues to supply vegetation with moisture through the dry season long after the soil moisture has been exhausted (Graham et al. 2010, Bales et al. 2011).

Decreasing moisture storage as erosion rates increase, thus reducing water availability in the dry season, provides a compelling explanation for the observed trends. Water availability influences the tree species that can grow successfully, their growth and turnover rates, susceptibility to fire, drought, and other disturbance, and ultimately the mean AGB of the resulting communities. Our results suggest that trees are less likely to become large in high-erosion-rate areas, and will be more vulnerable in drought years than those on lower-erosion-rate areas with enhanced soil and saprolite water availability. This conclusion is supported by the result that AGB was negatively correlated with temperature: drought sensitivity is increased by temperature (Adams et al. 2009), and clearly this negative effect here outweighs any positive effect of increased radiation for photosynthesis.

Crossing the erosion gradient in the Feather River region, the landscape becomes increasingly inhospitable. Both the less extensively weathered saprolite and loss of clay from the soil as erosion rates increase (Yoo et al. 2011) act to reduce the amount of water retained on the hillslope for ecological use, thus limiting forest productivity. The clear trends expressed in this landscape corroborate previous work elsewhere in the Sierra Nevada by Meyer et al. (2007), who noted that at the stand level, stand basal area was positively correlated with the combined thickness of the A and C horizons, which should obey an inverse relationship with erosion rate (Dixon et al. 2012).

In more humid settings, moisture limitation ceases to place such strong constraints on ecosystem productivity, and erosion rates are more tightly coupled to the bioavailability of key nutrients (e.g., Vitousek et al. 2003, Porder et al. 2005), though soil and saprolite water storage capacity has been implicated in explaining the vulnerability of trees to droughts even in normally very wet regions (Slik et al. 2002). At high erosion rates, it has been posited that productivity could be limited either by phosphorous limitation, due to a reduction in the weathering extent (Porder et al. 2007), or nitrogen limitation, due to nitrogen loss through more frequent landslides (Hilton et al. 2013). In these settings, it is likely that the relationship between erosion rate and the ecosystem properties may differ, depending on the pervasiveness and efficiency of chemical weathering, and the primary mechanisms by which erosion occurs. Exploring how climate modulates this relationship remains an important challenge for future work quantifying eco-geomorphological coupling.

These findings have important implications for understanding longer-term evolution of landscapes. By actively penetrating into bedrock, tree roots efficiently drive the physical formation of soil (Gabet and Mudd 2010, Roering et al. 2010). Larsen et al. (2014) postulated that the extremely high soil production rates they observed in the Western Alps of New Zealand, reaching 2.5 mm/yr, were possible as a consequence of persistent active bioturbation by plant roots, maintaining soil-mantled hillslopes at erosion rates reaching 10 mm/yr. In contrast, in the semiarid San Gabriel Mountains of southern California, where moisture limitation is important and vegetation is thus likely to be more strongly controlled by erosion rate, maximum observed soil production rates are 0.37 mm/yr, an order of magnitude lower than those reported from New Zealand (Heimsath et al. 2012).

CONCLUSIONS

In conclusion, empirical observations of AGB variations across a gradient of long-term erosion rates highlight geomorphic dynamics as a potentially important bottom-up control on the structural properties of the mixed-conifer forests of the northwestern Sierra Nevada Mountains. Specifically, increased erosion rates appear to be associated with lower AGB, a hitherto unconstrained relationship. In this setting, this relation-

ship can be rationalized as being driven by moisture limitation as a direct consequence of the corresponding reduction in soil and saprolite development. This relationship is likely to exist elsewhere, but its strength and mechanism is likely to vary according to the range of erosion rates, bedrock lithology, climate, and the presence and intensity of natural or anthropogenic disturbance. We suggest that consideration of the underlying geomorphic setting is therefore important to consider when investigating variations in forest characteristics across landscapes.

Acknowledgments

This research was funded by a NERC studentship (NERC DTG NE/152830X/1 and NE/J500021/1; D. T. Milodowski), in addition to the Harkness Award from the University of Cambridge (D. T. Milodowski). E. Mitchard is funded by a NERC Fellowship (NE/I021217/1).

Literature Cited

Adams, H. D., M. Guardiola-Claramonte, G. A. Barron-Gafford, J. C. Villegas, D. D. Breshears, C. B. Zou, P. A. Troch, and T. E. Huxman. 2009. Temperature sensitivity of drought-induced tree mortality portends increased regional die-off under global-change-type drought. Proceedings of the National Academy of Sciences USA 106:7063–7066.

Ahnert, F. 1970. Functional relationships between denudation, relief, and uplift in large mid-latitude drainage basins. American Journal of Science 268:243–263.

Asner, G. P., J. Mascaro, H. C. Muller-Landau, G. Vieilledent, R. Vaudry, M. Rasamoelina, J. S. Hall, and M. van Breugel. 2012. A universal airborne LiDAR approach for tropical forest carbon mapping. Oecologia 168:1147–1160.

Bales, R. C., J. W. Hopmans, A. T. O'Geen, M. Meadows, P. C. Hartsough, P. Kirchner, C. T. Hunsaker, and D. Beaudette. 2011. Soil moisture response to snowmelt and rainfall in a Sierra Nevada mixed-conifer forest. Vadose Zone Journal 10:786–799.

Chase, M. N., E. A. Johnson, and Y. E. Martin. 2012. The influence of geomorphic processes on plant distribution and abundance as reflected in plant tolerance curves. Ecological Monographs 82:429–447.

Chave, J., R. Condit, S. Aguilar, A. Hernandez, S. Lao, and R. Perez. 2004. Error propagation and scaling for tropical forest biomass estimates. Philosophical Transactions of the Royal Society B 359:409–420.

Chorover, J., et al. 2011. How water, carbon, and energy drive critical zone evolution: the Jemez–Santa Catalina critical zone observatory. Vadose Zone Journal 10:884–899.

Clubb, F. J., S. M. Mudd, D. T. Milodowski, M. D. Hurst, and L. J. Slater. 2014. Objective extraction of channel heads from high-resolution topographic data. Water Resources Research 50:4283–4304.

Daly, C., M. Halbleib, J. I. Smith, W. P. Gibson, M. K. Doggett, G. H. Taylor, J. Curtis, and P. P. Pasteris. 2008. Physiographically sensitive mapping of climatological temperature and precipitation across the conterminous United States. International Journal of Climatology 28:2031–2064.

Detto, M., H. C. Muller-Landau, J. Mascaro, and G. P. Asner. 2013. Hydrological networks and associated topographic variation as templates for the spatial organization of tropical forest vegetation. PLoS ONE 8:e76296.

Dixon, J. L., A. S. Hartshorn, A. M. Heimsath, R. A. DiBiase, and K. X. Whipple. 2012. Chemical weathering response to tectonic forcing: a soils perspective from the San Gabriel Mountains, California. Earth and Planetary Science Letters 323–324:40–49.

Franklin, J. 2003. Clustering versus regression trees for determining ecological land units in the Southern California mountains and foothills. Forest Science 49:354–368.

Gabet, E. J., and S. M. Mudd. 2010. Bedrock erosion by root fracture and tree throw: a coupled biogeomorphic model to explore the humped soil production function and the persistence of hillslope soils. Journal of Geophysical Research 115:F04005.

Gabet, E. J., O. J. Reichman, and E. W. Seabloom. 2003. The effects of bioturbation on soil processes and sediment transport. Annual Review of Earth and Planetary Sciences 31:249–273.

Gilbert, G. 1909. The convexity of hilltops. Journal of Geology 17:344–350.

Gonzalez, P., G. P. Asner, J. J. Battles, M. A. Lefsky, K. M. Waring, and M. Palace. 2010. Forest carbon densities and uncertainties from Lidar, QuickBird, and field measurements in California. Remote Sensing of Environment 114:1561–1575.

Goulden, M. L., R. G. Anderson, R. C. Bales, A. E. Kelly, M. Meadows, and G. C. Winston. 2012. Evapotranspiration along an elevation gradient in California's Sierra Nevada. Journal of Geophysical Research—Biogeosciences 117: G03028.

Graham, R., A. Rossi, and R. Hubbert. 2010. Rock to regolith conversion: producing hospitable substrates for terrestrial ecosystems. GSA Today 20(2):4–9.

Heimsath, A. M., R. A. DiBiase, and K. X. Whipple. 2012. Soil production limits and the transition to bedrock-dominated landscapes. Nature Geoscience 5:210–214.

Heimsath, A., W. Dietrich, K. Nishiizumi, and R. Finkel. 1997. The soil production function and landscape equilibrium. Nature 388:358–361.

Hilton, R. G., A. Galy, A. J. West, N. Hovius, and G. G. Roberts. 2013. Geomorphic control on the $\delta^{15}N$ of mountain forests. Biogeosciences 10:1693–1705.

Hubbert, K. R., R. C. Graham, and M. A. Anderson. 2001. Soil and weathered bedrock. Soil Science Society of America Journal 65:1255–1262.

Hurst, M. D., S. M. Mudd, R. Walcott, M. Attal, and K. Yoo. 2012. Using hilltop curvature to derive the spatial distribution of erosion rates. Journal of Geophysical Research—Earth Surface 117:F02017.

Hurst, M. D., S. M. Mudd, K. Yoo, M. Attal, and R. Walcott. 2013. Influence of lithology on hillslope morphology and response to tectonic forcing in the northern Sierra Nevada of California. Journal of Geophysical Research—Earth Surface 118:832–851.

Jenkins, J. C., D. C. Chojnacky, L. S. Heath, and R. A. Birdsey. 2003. National-scale biomass estimators for United States tree species. Forest Science 49:12–35.

Kirkby, M. J. 1985. A basis for soil profile modelling in a geomorphic context. Journal of Soil Science 36:97–121.

Larsen, I. J., P. C. Almond, A. Eger, J. O. Stone, D. R. Montgomery, and B. Malcolm. 2014. Rapid soil production and weathering in the Southern Alps, New Zealand. Science 343:637–640.

Lefsky, M. A., D. Harding, W. Cohen, G. Parker, and H. Shugart. 1999. Surface Lidar remote sensing of basal area and biomass in deciduous forests of eastern Maryland, USA. Remote Sensing of Environment 67:83–98.

Mascaro, J., M. Detto, G. P. Asner, and H. C. Muller-Landau. 2011. Evaluating uncertainty in mapping forest carbon with airborne LiDAR. Remote Sensing of Environment 115:3770–3774.

Meyer, M., M. North, A. Gray, and H. Zald. 2007. Influence of soil thickness on stand characteristics in a Sierra Nevada mixed-conifer forest. Plant and Soil 294:113–123.

Miller, J. D., and A. E. Thode. 2007. Quantifying burn severity in a heterogeneous landscape with a relative version of the

delta normalized burn ratio (dNBR). Remote Sensing of Environment 109:66–80.
Montgomery, D., and M. Brandon. 2002. Topographic controls on erosion rates in tectonically active mountain ranges. Earth and Planetary Science Letters 201:481–489.
Mudd, S. M., and K. Yoo. 2010. Reservoir theory for studying the geochemical evolution of soils. Journal of Geophysical Research—Earth Surface 115:F03030.
Návar, J. 2009. Allometric equations for tree species and carbon stocks for forests of northwestern Mexico. Forest Ecology and Management 257:427–434.
Porder, S., A. Paytan, and P. M. Vitousek. 2005. Erosion and landscape development affect plant nutrient status in the Hawaiian Islands. Oecologia 142:440–449.
Porder, S., P. Vitousek, O. Chadwick, C. Chamberlain, and G. Hilley. 2007. Uplift, erosion, and phosphorus limitation in terrestrial ecosystems. Ecosystems 10:159–171.
Riebe, C. S., J. W. Kirchner, D. E. Granger, and R. C. Finkel. 2000. Erosional equilibrium and disequilibrium in the Sierra Nevada, inferred from cosmogenic ^{26}Al and ^{10}Be in alluvial sediment. Geology 28:803–806.
Riebe, C. S., J. W. Kirchner, D. E. Granger, and R. C. Finkel. 2001. Minimal climatic control on erosion rates in the Sierra Nevada, California. Geology 29:447–450.
Roering, J. J., J. W. Kirchner, and W. E. Dietrich. 1999. Evidence for nonlinear, diffusive sediment transport on hillslopes and implications for landscape morphology. Water Resources Research 35:853–870.
Roering, J., J. Kirchner, L. Sklar, and W. Dietrich. 2001. Hillslope evolution by nonlinear creep and landsliding: an experimental study. Geology 29:143–146.
Roering, J. J., J. Marshall, A. M. Booth, M. Mort, and Q. Jin. 2010. Evidence for biotic controls on topography and soil production. Earth and Planetary Science Letters 298:183–190.
Saucedo, G. J., and D. L. Wagner. 1992. Geologic map of the Chico quadrangle. California Division of Mines and Geology, Sacramento, California, USA.
Slik, J. W. F., R. W. Verburg, and P. J. A. Kessler. 2002. Effects of fire and selective logging on the tree species composition of lowland dipterocarp forest in East Kalimantan, Indonesia. Biodiversity and Conservation 11:85–98.
Stephenson, N. L. 1998. Actual evapotranspiration and deficit: biologically meaningful correlates of vegetation distribution across spatial scales. Journal of Biogeography 25:855–870.
Urban, D. L., C. Miller, P. N. Halpin, and N. L. Stephenson. 2000. Forest gradient response in Sierran landscapes: the physical template. Landscape Ecology 15:603–620.
Vanwalleghem, T., U. Stockmann, B. Minasny, and A. B. McBratney. 2013. A quantitative model for integrating landscape evolution and soil formation. Journal of Geophysical Research: Earth Surface 118:331–347.
Vitousek, P., O. Chadwick, P. Matson, S. Allison, L. Derry, L. Kettley, A. Luers, E. Mecking, V. Monastra, and S. Porder. 2003. Erosion and the rejuvenation of weathering-derived nutrient supply in an old tropical landscape. Ecosystems 6: 762–772.
Warton, D. I., I. J. Wright, D. S. Falster, and M. Westoby. 2006. Bivariate line-fitting methods for allometry. Biological Reviews 81:259–291.
Witty, J. H., R. C. Graham, K. R. Hubbert, J. A. Doolittle, and J. A. Wald. 2003. Contributions of water supply from the weathered bedrock zone to forest soil quality. Geoderma 114: 389–400.
Yanai, R. D., J. J. Battles, A. D. Richardson, C. A. Blodgett, D. M. Wood, and E. B. Rastetter. 2010. Estimating uncertainty in ecosystem budget calculations. Ecosystems 13:239–248.
Yoo, K., B. Weinman, S. M. Mudd, M. Hurst, M. Attal, and K. Maher. 2011. Evolution of hillslope soils: the geomorphic theater and the geochemical play. Applied Geochemistry 26: S149–S153.

Supplemental Material

Ecological Archives

The Appendix is available online: http://dx.doi.org/10.1890/14-0649.1.sm

Reports